land

Supplementary Materials

Effects of tree shade on vineyard microclimate and grape production: a novel approach to sun radiation modeling as a response to climate change

Isilda Cunha Menezes [1], Mário Santos [2,3,4,*], Lourdes Bugalho [5] and Mário Gonzalez Pereira [4,6]

[1] Center for Environmental and Marine Studies (CESAM), Department of Environment and Planning, University of Aveiro, Campus Universitário de Santiago, Aveiro, Portugal; isildacm@ua.pt

[2] Laboratory of Fluvial and Terrestrial Ecology (LEFT), Innovation and Development Center and Department of Biology and Environment, University of Trás-os-Montes e Alto Douro, Vila Real, Portugal; mgsantos@utad.pt

[3] Research Group on Ecology and Conservation of Amazonian Biodiversity, Campus Itaituba, Federal Institute of Education, Science and Technology of Para, Itaituba, PA, Brazil; mgsantos@utad.pt

[4] Centre for the Research and Technology of Agro-Environment and Biological Sciences (CITAB), Institute for Innovation, Capacity Building and Sustainability of Agri-food Production (Inov4Agro), Vila Real, Portugal; mgsantos@utad.pt, gpereira@utad.pt

[5] Portuguese Institute for Sea and Atmosphere (IPMA), Department of Meteorology and Geophysics, Lisboa, Portugal; lourdes.bugalho@ipma.pt

[6] Institute Dom Luiz (IDL), University of Lisbon, Lisbon, Portugal; gpereira@utad.pt

* Correspondence: mgsantos@utad.pt

1. Summary

A detailed description of the Integrated Model of Vitiforestry and Adaptation to Climate Change (IMVSCA) is presented here. First, Section 2 presents a general description of IMVSCA, including its main components (modules and submodules), its objectives, and a list of its input and output variables and parameters. The following sections describe each of the different IMVSCA components in detail. Finally, the interactions between the various components are explained.

2. IMVSCA overview

The IMVSCA aims to simulate the role of different factors, especially meteorological and climate drivers, in vineyard and viticulture production systems. Consequently, IMVSCA is not just a singular model with a single objective, but a modeling system composed of several simple models, each with its objective. These simple models are called submodules and are organized/grouped into modules. The IMVSCA system comprises four modules with the following general objectives:

• The Light–Shadow module aims to assess the shading effect of a single tree on a grapevine or of an orchard on a vineyard;

• The Phenology module aims to evaluate seasonal and cyclical phenomena, such as budburst, flowering, veraison, maturity, and chilling as a function of meteorological conditions and other environmental factors;

• The Zoning module aims to evaluate the suitability of a site for viticulture;

• The Illness module aims to evaluate the occurrence of common grapevine diseases.

Each of the modules is made up of several submodules, each with its objective. The Light–Shadow module includes three submodules: *Sunrise–Sunset*, *Tree–Shadow*, and *Light–Orchard*. As the names suggest, the *Sunrise–Sunset submodule* calculates the sunrise and sunset hours. The *Tree–Shadow submodule* computes the shadow effect of a tree on the vine, estimating the mean air temperature and relative humidity near the grapevine when exposed to sunlight and under the shadow of trees, based on the daily periods of shadow

and sunlight passing around the treetop. The *Light–Orchard submodule* estimates the photosynthetically active radiation (PAR) received by the vineyards in sunny or shaded conditions, for a defined orchard configuration, based on the daily period during which the vineyard is influenced by sunlight passing through the tree gaps.

The Phenology module monitors and predicts the developmental stages of grapevines. It utilizes meteorological data to model the timing of these phenological phases. This module aids in optimizing vineyard management practises to improve grape quality and yield. The Zoning module assesses climatic conditions and their influence on grapevine development, quantifying the mean thermal amplitude during the maturation periods. It also considers hydrologic balance and potential evapotranspiration to estimate the potential sugar content in grapes. Additionally, it includes the growing season suitability and precipitation during the growing season. The Illness module assesses the risk of powdery mildew infection in the grapevines based on the risk assessment model developed by the University of California, Davis [1]. It uses meteorological data to predict the favorable conditions for pathogen infection and growth. It also determines the primary and secondary downy mildew infections, quantifying the delay or advancement of outbreaks.

The remainder of this document provides the complete formulation of the IMVSCA model system. Table S1 lists the acronyms, definitions, and units of the variables used in these formulations, as well as the parameterization values adopted in this research.

Table S1. List of symbols.

Variable	Meaning	Units
B_{hidri}	Hydric balance from September to August	mm
d_a	Year number of days	
d_n	Number of days of the year, starting from January 1	
E_t	Monthly potential transpiration in the vineyard	mm
E_s	Monthly soil direct evaporation	mm
ETP	Evapotranspiration	$mm\,day^{-1}$
Flor	Number of days from January 1 to flowering	
$H_{obs,D}$	Daily global solar radiation	$MJm^{-2}day^{-1}$
HR	Relative humidity of air	%
h_{tree}	Tree height	m
l_d	Day length coefficient for the local latitude	1.02
I_{sc}	Solar constant	118.108 $MJm^{-2}day^{-1}$
L	Leaf Area Index (LAI) of the canopy	m^2m^{-2}
N	Number of days per month	
$N_{ef\,prec}$	Number of days of effective evaporation from the soil per month	
$N_{Verai-Matu}$	Number of days from veraison to maturation	
P_a	Surface pressure	kPa
P_d	Daily accumulated precipitation	mm
PET	Monthly total potential evapotranspiration	mm
P_m	Monthly accumulated precipitation	mm
T_b	Base daily mean air temperature (10ºC)	°C
T_w	Daily dew point temperature	°C
T	Daily mean air temperature	°C

$T_{Verai-Matu}$	Daily mean air temperature from veraison to maturation.	°C
k	Coefficient of radiation absorption	
T_{max}	Daily maximum air temperature	°C
T_{min}	Daily minimum air temperature	°C
t	Hours recorded in a 24-hour format	h
t_{sr}	Time of solar sunrise	h
t_{ss}	Time of solar sunset	h
W_0	Initial useful soil water reserve	$200\ mm$
W	Wind speed	ms^{-1}
x	The ratio of the average projected area of the tree crown	1
α	Solar elevation angle	rad
α_t	Constant azimuth angle of the tree trunk	rad
ψ	Solar azimuth angle	rad
δ	Solar declination angle	rad
ϕ	Geographic latitude positive towards the north	rad
β	Geographic longitude positive towards the east	°
γ	Terrain slope	°
ρ	Ground aspect	°

3. Light–Shadow Module

3.1. The Sunrise–Sunset submodule

In this submodule, the sunrise and sunset hours are calculated using the formulation of Nasrin et al. [2]. In detail, this module determines the number of days (*n*, Equation S5) since January 1st, 2000, 12:00 based on the Julian date (*JD*, Equation S4), the solar mean anomaly (M (°), Equation S6), the equation of the center (C, Equation S7), the ecliptic longitude (λ (°), Equation S8), the solar transit (Jtransit, Equation S9), the solar declination (δ (°), Equation S10), the hour angle (ω (°), Equation S11), and finally, the actual Julian date of sunrise (Equation S13) and sunset (Equation S12).

$$a = int((14 - month)/12) \tag{S1}$$

$$y = year + 4800 - a \tag{S2}$$

$$m = month + 12 * a - 3 \tag{S3}$$

$$
\begin{aligned}
JD = &\ day + int((153 * m + 2)/5) + 365 * y + int(y/4) - int(y/100) \\
&+ int(y/400) - 32045 + (hour - 12)/24 + minute/1440 \\
&+ second/86400
\end{aligned}
\tag{S4}
$$

$$n = int\left(JD - 2451545.0009 - \frac{\beta}{360} + 1/2\right) \tag{S5}$$

$$
M = \left(357.5291 + 0.98560028\left(2451545.0009 + \frac{\beta}{360} + n \right.\right.
$$
$$
\left.\left. - 2451545\right)\right) mod\, 360
\tag{S6}
$$

$$C = 1.9148 * \sin(M) + 0.02 * \sin(2M) + 0.0003 * \sin(3M) \tag{S7}$$

$$\lambda = (M + 102.9372 + C + 180)mod360 \tag{S8}$$

$$Jtransit = 2451545.0009 + \frac{\beta}{360} + n + 0.0053sin(M) - 0.0069 * sin(2\lambda) \tag{S9}$$

$$\delta = 57.29577951\left(arcsen(\sin(\lambda)\sin(23.45))\right) \tag{S10}$$

$$w = 57.29577951\left(arccos\left(\frac{\sin(-0.83) - sin(\phi)sin(\sin(\lambda)\sin(23.45))}{cos(\phi)cos(\delta)}\right)\right) \tag{S11}$$

$$Sunset = 2451545.0009 + \frac{(\omega + \beta)}{360} + n + 0.0053(sin(M)) - 0.0069(sin(2\lambda)) \tag{S12}$$

$$Sunrise = Jtransit - (Sunset - Jtransit) \tag{S13}$$

Then, the submodule converts the Julian date of sunrise and sunset into a calendar date [3,4], as follows:

$$timefromJD(time) = time + 0.5 \ \text{ with } \ time = Sunrise \ or \ Sunset \tag{S14}$$

$$secs = int(int(time - int(time)) * 24 * 60 * 60 + 0.5) \tag{S15}$$

$$mins = int\left(\frac{secs}{60}\right) \tag{S16}$$

$$hour = int\left(\frac{mins}{60}\right) \tag{S17}$$

3.2. The Tree–Shadow submodule

This model incorporates some formulations based on Hu et al. [5] for solar radiation. Specifically, it uses the daily hour angle (ω_h(radians), Equation S18, zero at noon and positive in the morning), and the solar elevation angle at solar noon (α, Equation S20) relative to the equatorial plane and local latitude. This last parameter along with the solar azimuth angle (ψ, Equation S21) and the sunrise hour angle (ω_s (°), Equation S23), are calculated using the solar declination (δ (radians), Equation S10) simulated by the *Sunrise–Sunset submodule*. Additionally, the model calculates the day angle (Γ (radians), Equation S19), the eccentricity correction factor of the Earth's orbit (E_0, Equation S22), the daily extraterrestrial radiation (H_0 ($MJm^{-2}day^{-1}$), Equation S24), and the maximum possible daily sunshine duration (S_0 (hours), Equation S25).

The sunshine duration (SD) is a ratio derived from the potential sunshine duration (PSD), the maximum possible daily sunshine duration (S_0) as given by Equation S26, and the monthly average daily SD observed from station data on a horizontal surface (S in hours). Then, the Angstrom–Prescott model [6] (Equation S29) was used to calculate the ratio H/H_0, as a function of S, to determine the daily global radiation (H) for the period between the sunrise and the sunset.

$$\omega_h = (t - 12)\,\frac{\pi}{12} \tag{S18}$$

$$\Gamma = 2\pi\,\frac{d_n - 1}{d_a} \tag{S19}$$

$$sen\alpha = sen\delta\,sen\phi + cos\delta\,cos\phi\,cos\omega_h \tag{S20}$$

$$cos\psi = \frac{sen\delta\,cos\phi - cos\delta\,cos\omega_h\,sen\phi}{cos\alpha} \tag{S21}$$

$$E_0 = 1.000110 + 0.034221\,cos\Gamma + 0.001280\,sen\Gamma + 0.000719\,cos2\Gamma \\ + 0.000077\,sen2\Gamma \tag{S22}$$

$$\omega_s = arccos(-tg\phi\,tg\delta) \tag{S23}$$

$$H_0 = \frac{1}{\pi}\,I_{sc}\,E_0\,\left(\frac{\pi}{180}\,\omega_s\,sen\delta\,sen\phi + cos\delta\,cos\phi\,sen\omega_s\right) \tag{S24}$$

$$S_0 = \frac{2}{15}\,\omega_s \tag{S25}$$

$$SD = PSD\,\frac{S}{S_0} \tag{S26}$$

$$a = -0.309 + 0.539\,cos\phi - 0.0693\,h + 0.290\,\frac{S}{S_0} \tag{S27}$$

$$b = 1.527 - 1.027\,cos\phi + 0.0926 - 0.359\,\frac{S}{S_0} \quad \text{where } h \text{ is the elevation } (km) \tag{S28}$$

$$\frac{H}{H_0} = a + b\,\frac{S}{S_0} \tag{S29}$$

Complementary formulations developed by the paper's author to calculate the shadow over the vineyards, and the mean air temperature surrounding the vineyard based on Hargreaves and Samani [7], are described in Section 2.2.1.2. In this document (Supplementary Materials), the calculation of the relative humidity of the air is detailed in subsection 3.3, "*Supplementary calculations made by the model*". This calculation is performed using the mean air temperature provided by this submodule and the virtual air temperature supplied by observations. Because the paper associated with these Supplementary Materials presents a study considering flat terrain without any interactions, such as trees, no formulations related to topographic interactions given by the slope (γ) and aspect (ρ) of the ground are presented.

3.3. Supplementary calculations made by the model

In the *Tree–Shadow submodule*, the relative humidity *RH* (%) is calculated using Equation S30 from Doorenbos and Pruitt [8]. This Equation provides the best fit with the observed meteorological station series for Portugal, as described by Castellví et al. [9], and can be used at hourly or daily time steps. This equation represents the ratio of actual vapor pressure to equilibrium vapor pressure (e_a (kPa), Equation S31) at a given temperature, and saturation vapor pressure (e_s (kPa), Equation S32). Both of the parameters were calculated using the formulation described in Zotarelli et al. [10].

$$RH = 100\,\frac{e_a\,(T_w)}{e_s\,(T)} \tag{S30}$$

$$e_s = 0.6108 \left(exp^{\frac{17.27\,T}{237.3+T}} \right) \hspace{3cm} \text{S31}$$

$$e_a = 0.6108 \left(exp^{\frac{17.27\,T_w}{237.3+T_w}} \right) \hspace{3cm} \text{S32}$$

3.4. Light–Orchard submodule

This submodule calculates photosynthetically active radiation (PAR) using the formulation by Oyarzun et al. [11]. This calculation is based on the proportion of the orchard floor shaded by trees at any given time. This model has been tested only for near-continuous hedgerow situations and was implemented in this submodule due to its similarity to the organization of vineyard plantations (Figure S1).
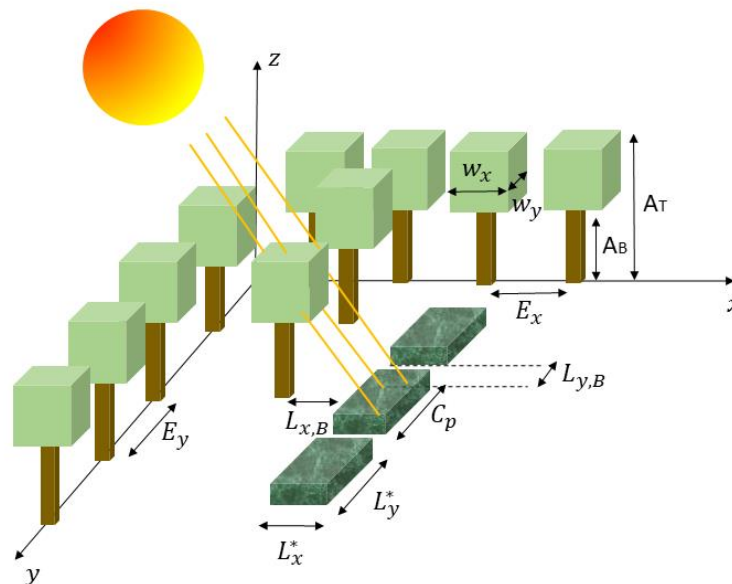

Figure S1. Schematic representation of a fruit-tree orchard showing the model input variables related to orchard configuration [11].

This model uses the solar azimuth angle (ψ, Equation S21), the solar elevation angle (α, Equation S20) at a given hour, the daily extraterrestrial radiation (H_0, Equation S24), and the daily global radiation (H (MJ.m^{-2}.day^{-1}), Equation S29) simulated by the *Tree–Shadow submodule* to calculate the hourly extraterrestrial solar radiation ($H_{0,h}$ (Wm^{-2}), Equation S33), and the hourly incident global solar irradiance ($H_{s,h}$ (Wm^{-2}), Equation S34).

Additionally, the submodule calculates the hourly diffuse incoming radiation ($H_{d,h}$ (Wm^{-2}), Equation S35) as a function of atmospheric transmittance (τ, Equation S36) and optical air mass number (m, Equation S37) [12]. The submodule also determines the hourly beam solar irradiance ($H_{b,h}$ (Wm^{-2}), Equation S38), the hourly fraction of beam solar radiation ($F_{H_{b,h}}$, Equation S39), and the diffuse solar radiation ($F_{H_{d,h}}$, Equation S40). It is assumed that the fractions of direct (beam) and diffuse radiation within the photosynthetically active radiation (PAR) range ($F_{PAR_{b,h}}$(Equation S39) and $F_{PAR_{d,h}}$ (Equation S40)) are

the same as the proportions present in the entire solar radiation spectrum, covering all wavelength ranges.

Since the hourly beam solar irradiance $H_{b,h}$ and hourly diffuse incoming radiation $H_{d,h}$ are projected onto a horizontal surface, they were corrected for the slope of terrain using the sun view factor (w_f) for diffuse radiation (Equation S44) and the topographic effect (σ) for solar irradiation (Equation S42). Consequently, the actual amount of radiation received by the sloped surface is $H_{g,h}^*$ (Equation S45).

$$H_{0,h} = 1360\ cos\alpha \tag{S33}$$

$$H_{s,h} = \frac{H_{0,h}\ H}{H_0} \tag{S34}$$

$$H_{d,h} = 0.3(1 - \tau^m)H_{0,h} \tag{S35}$$

$$\tau = \frac{H}{H_0} \tag{S36}$$

$$m = \frac{P_a}{101.3\ \cos\alpha} \tag{S37}$$

$$H_{b,h} = H_{s,h} - H_{d,h} \tag{S38}$$

$$F_{H_{b,h}} = \frac{H_{b,h}}{H_{s,h}} = F_{PAR_{b,h}} \tag{S39}$$

$$F_{H_{d,h}} = \frac{H_{d,h}}{H_{s,h}} = F_{PAR_{d,h}} \tag{S40}$$

$$H_{b,h}^* = H_{b,h}\ \sigma \tag{S41}$$

$$\sigma = \frac{cos(\gamma)\ cos(\alpha) + sen(\gamma)sen(\alpha)\ cos(\psi - \rho)}{cos(\alpha)} \tag{S42}$$

$$H_{d,h}^* = H_{d,h}\ w_f \tag{S43}$$

$$w_f = \frac{1 + cos(\gamma)}{2} \tag{S44}$$

$$H_{g,h}^* = H_{b,h}^* + H_{d,h}^* \tag{S45}$$

The calculation of fractional radiation interception is based on the proportion of the orchard ground that is shaded by the trees at any given hour of the day. According to Figure S1 [11], and assuming that the canopy extends to the soil surface (with no bare stem portion), the maximum length of the shadow cast by the trees can be determined perpendicular to the row (L_x (m), Equation S46), and along the row (L_y (m), Equation S47). However, corrections must be considered, especially for the bare trunk portion of the trees, which casts a less significant shadow length (m), allowing more radiation to reach the orchard floor at certain hours of the day. Thus, the blank shadow length (m) is calculated both perpendicular to the row ($L_{x,B}$) and along the row ($L_{y,B}$) (Figure S1), using Equations S46 and S47, but with the height of tree base (A_B) instead of the total height of the tree (A_T). A correction factor (θ), accounting for the combined effects of the sun zenith angle, terrain slope, and aspect, is used to calculate the effective shadow length cast by the trees

perpendicular to the row (L_x^*, Equation S48) and along the row (L_y^*, Equation S49). The fraction of the orchard floor that is shaded at any hour is then obtained by $f_{l,h}$ (Equation S51), based on L_x^* and L_y^*, as well as the canopy dimensions (W_x and W_y) and the distance between the trees (E_x and E_y).

$$L_x = A_T[tg(\alpha)\, sen(\psi - \alpha_t)] \tag{S46}$$

$$L_y = A_T[tg(\alpha)\, cos(\psi - \alpha_t)] \tag{S47}$$

$$L_x^* = \left(L_x - L_{x,B}\right)\theta \tag{S48}$$

$$L_y^* = \left(L_y - L_{y,B}\right)\theta \tag{S49}$$

$$\theta = \begin{cases} cos(\gamma) & 45° < (\psi - \rho) < 135° \\ \frac{1}{cos(\gamma)} & 225° < (\psi - \rho) < 315° \\ 1 & otherwise \end{cases} \text{, with } \psi \text{ in } ° \tag{S50}$$

$$f_{l,h} = \frac{\left[(L_x^* + W_x)W_y + \left(L_y^* + W_y\right)W_x\right] - \left(W_x W_y\right)}{E_x E_y} \tag{S51}$$

The beam radiation interception ($f_{b,h}$, Equation S52) on an orchard basis is calculated for each hour of the day. The transmission of light through the leaves depends on the range of the sun's zenith angles, the canopy architectures, and the leaf absorptivity values. The tree's effective canopy porosity (C_p^*, Equation S53) is a function of the sun fleck fraction on the orchard ground shadowed area or the canopy extinction coefficient (C_p, Equation S54) and the leaf absorptivity coefficient (μ). The coefficient $\mu = 1$ for black leaves, and when μ is small, the radiation will be minimally attenuated. Canopies typically have absorptivity values of $\mu = 0.8$ for PAR and $\mu = 0.2$ for NIR radiation. For total solar radiation, the absorptivity is the mean of the values for PAR and NIR, $\mu = 0.5$ [12].

Following Campbell and Norman [12], the effects of leaf spectral properties are separated from the effects of canopy architecture because most leaves have similar reflectance and transmittance spectra, even though they depend on wavelength. However, canopy architecture can vary widely with species, environmental conditions, and time, thereby providing an additional amount of radiation under the canopy. Thus, the canopy extinction coefficient (C_p) requires the calculation of the area average projection from some direction onto the horizontal. If all of the leaves in a canopy are vertical but with random azimuthal orientations, then for the distribution of thw canopy area projected onto the horizontal of a hemi-surface area cylinder, this coefficient is $K_{b1,\alpha}$ (Equation S55). A canopy might have leaves with leaf inclination angles similar to the distribution of angles on the surface of a sphere.

Then, the extinction coefficient, calculated from the ratio of the projected hemi-surface area sphere, is $K_{b2,\alpha}$ (Equation S56). The ellipsoidal distribution generalizes the spherical, allowing the sphere to be flattened or elongated. An extinction coefficient for the ratio of the projected ellipsoid hemi-surface area [13] is $K_{b3,\alpha}$ (Equation S57).

$$f_{b,h} = f_{l,h}\left(1 - C_p^*\right) \tag{S52}$$

$$C_p^* = e^{\left(ln(C_p)\sqrt{\mu}\right)} \tag{S53}$$

$$C_p = K_{b,\alpha}\, L \tag{S54}$$

with $\ K_{b,\alpha} = K_{bi,\alpha}\ , i = 1,3$

$$K_{b1,\alpha} = \frac{2\,tg\alpha}{\pi} \tag{S55}$$

$$K_{b2,\alpha} = \frac{1}{2\,cos\alpha} \tag{S56}$$

$$K_{b3,\alpha} = \frac{\sqrt{x^2 + (tg\alpha)^2}}{x + 1.774\,(x + 1.182)^{-0.733}} \tag{S57}$$

with x as the ratio of the average projected area of the tree crown $x = 1$, for a spherical leaf angle distribution; $x = 0$, for a vertical distribution; and $x \to \infty$, for a horizontal leaf canopy.

Then, the orchard-based beam transmittance for each hour is $\tau_{b,h}$ (Equation S58), and the daily averaged effective orchard diffuse transmittance is $\tau_{d,D}$ (Equation S59). Thus, we can determine the diffuse radiation interception fraction for the orchard ($f_{d,D}$, Equation S60). Finally, the hourly fractional PAR interception is obtained through $f_{IPAR,h}$ (Equation S61), and the daily PAR interception fraction is obtained as f_{DIPAR} (Equation S62) through PAR_h (Equation S63).

$$\tau_{b,h} = 1 - f_{b,h} \tag{S58}$$

$$\tau_{d,D} = 2\sum_{h=t_{sr}+1}^{h=t_{ss}}\left(\tau_{b,h}\,cos(\alpha_h)\,sen(\alpha_h)\,d\alpha_{h-(h-1)}\right) \tag{S59}$$

$$f_{d,D} = 1 - \tau_{d,D} \tag{S60}$$

$$f_{IPAR,h} = f_{b,h}F_{PAR_{b,h}} + f_{d,D}F_{PAR_{d,h}} \tag{S61}$$

$$f_{DIPAR} = \frac{\sum_{h=t_{sr}+1}^{h=t_{ss}}\left(F_{IPAR,h}\,PAR_h\right)}{\sum_{h=t_{sr}+1}^{h=t_{ss}}PAR_h} \tag{S62}$$

$$PAR_h = H_{g,h}^*F_{PAR/H_g} \tag{S63}$$

with $F_{PAR/H_g} = 0.5$ being the fraction of H_g that corresponds to the PAR wavelength range. For the time of sunrise and sunset (t_{sr}, t_{ss}), we used the actual Julian date of sunrise and sunset simulated by the *Sunrise–Sunset submodule*.

4. Phenology Module

This module employs the chilling days model (*CH*, Equation (S64)) [14]. This model calculates the daily sum of the chilling rates (R_c), using an optimal chilling daily mean air temperature $\ T_0 = 6°C$ [15]. In Equation S65, the numerical values are calibrated based on Hanninen [16] and Sarvas [17].

$$CH = \sum_{t=0}^{t_n} R_c(T) \geq F \tag{S64}$$

$$R_c(T) = \begin{cases} 0 & T \leq -3.4 \\ (T + 3.4)/(T_0 + 3.4) & -3.4 < T < T_0 \\ (T - 10.4)/(T_0 - 10.4) & T_0 < T < 10.4 \\ 1 & T \geq 10.4 \end{cases} \tag{S65}$$

In the Phenology module, the onset of vegetative growth is determined by the first sequence of 5 consecutive days with a $T > 10°C$ threshold of vegetative zero [18].

Empirical Growing Degree–Days (GDD) models (FV, Equations (S66)) [19] were implemented in the Phenology module. A $T_0 = 3.5°C$ is used for budburst, and for flowering, veraison, and maturity, a $T_0 = 10°C$ is applied. In these models, the critical forcing state (F) was adjusted according to Lopes et al. [20] for the white grape varieties *Alvarinho, Antão Vaz, Arinto, Avesso, Bical, Ratinho, Chardonnay, Encruzado, Fernão Pires, Fonte Cal, Gouveio, Loureiro, Malvasia Fina, Moscatel Graúdo, Rabigato, Sercial, Siria, Verdelho,* and *Viosinho,* and for the red varieties *Alfrocheiro, Aragonez, Baga, Castelão, Cabernet Sauvignon, Jaen, Ramsico, Rufete, Tinta Barroca, Tinta Caiada, Tinto Cão, Touriga Franca, Touriga Nacional, Trincadeira,* and *Vinhão.* For these varieties, the budburst was analyzed after January 1st; while flowering, the budburst was analyzed after the first day of bud growth, the veraison was analyzed after the first day of flowering, the maturity was analyzed after the first day of veraison, and the chilling was analyzed after the first day of maturity.

Additionally, this module uses the GDD model from Parker et al. [21], which starts on the 60th day of the year. This model employs a $T_0 = 0°C$ and Parker et al.'s [21] calibration to determine the critical state. This model simulated the onset of flowering and veraison for other grape varieties, including the rosé grape *Pinot Gris* and *Gewurztraminer,* the red varieties *Cabernet Franc,* Syrah, and *Sangiovese,* and the white varieties *Riesling* and *Viognier.*

$$FV = \sum_{t=0}^{t_n} R_{f,v}(T) \geq F \tag{S66}$$

$$R_{f,v}(T) = \begin{cases} 0 & T \leq T_0 \\ T - T_0 & T > T_0 \end{cases} \tag{S67}$$

This Phenological module also accounts for episodes of frost (Table S2) that constitute an important risk to be managed by winegrowers, as it can cause significant damage to grapevines and very large losses, including the complete loss of grape production in a season [22]. Frost can be advective, black and radiative, or white [23,24]. Advective frost is associated with large-scale incursions of cold air, accompanied by strong wind, even during the daytime. Radiative frost is associated with cooling due to the energy loss through an exchange in temperature during a clear sky day, with calm night wind, and temperature inversions, i.e., when the temperature increases with the height [25,26] . In some cases, a combination of advective and radiation frost can occur [27], causing vegetation to burn via frost/freezing.

Radiative frosts are more frequent in the winter, but can also occur in the spring and autumn when they might damage the grapevines [28]. Unlike white frost, black frost has high destructive potential and can cause a great loss of yield and an economic impact [29]. In mainland Portugal, the risk of frost (advection frosts or black frosts, evaporation frosts

and irradiation frosts, or white frosts) is generally low throughout the territory but varies from medium to very high in the NE region (SNAA, 2012). This frost assessment was implemented in the module after the budburst started, following the recommendation of Poling [23,29] and Perry [30].

Table S2. Types of frost implemented in the Phenology module.

Frost	Temperature of air	Relative Humidity of	Wind Speed
White frost	$-2.2°C < T < 2.2°C$	$RH = 100\%$	
Frost/freeze	$T < -2.2°C$	$RH < 70\%$	$2.2ms^{-1} < W < 4.5ms^{-1}$
Black frost	$T < -2.2°C$	$RH < 70\%$	$W > 4.5ms^{-1}$

In addition to these events, this module analyzes days with conditions that are favorable for flowering [31] (Table S3), and optimal pollen spread [31,32]. It also considers the favorable conditions for pollen germination and fertilization, where fertilization can occur within 12 hours [31].

Table S3. Conditions favorable for flowering and pollination in the Phenology module.

Flowering process	Ranges	
Conditions for flowering	$15°C ≤ T ≤ 23°C \ and \ 28°C ≤ T$	
Optimal for flowering	$24°C ≤ T ≤ 27°C$	
Optimal pollen spread condi-	$18°C ≤ T ≤ 22°C$	$RH < 65\%$
Favorable conditions for pollen germination and fertilization	$25°C ≤ T ≤ 28°C$	

Furthermore, this module analyzes the favorable meteorological conditions for scalds in grapes, indicated by a threshold of $T_{max} > 38°C$ on days with $RH < 30\%$. It also examines the extreme precipitation events ($P > 18 \ mm$) occurring after the start of flowering.

This module also calculated evapotranspiration (ETP) using the research by Zotarelli et al. [10] detailing the two processes of water loss from the land surface to the atmosphere: evaporation and transpiration. Evaporation refers to the transformation of liquid water into water vapor (vaporization) and its removal from sources such as soil surfaces, wet vegetation, pavements, and water bodies. Transpiration involves the vaporization of liquid water within plants and the subsequent release of water vapor.

5. Zoning Module

This module infers the Dryness index, the Heliothermal Index of Huglin, the Cool Night indices from the Geoviticulture Multicriteria Climatic Classification System by Tonietto and Carbonneau [33], and the Cool Night Quality Bioclimatic Index [34]. It quantifies the mean air thermal amplitude during the maturation period and includes the

Hydrothermal Index of Branas [35], the Growing Season Suitability Index [36], and the Growing Season Precipitation Index [37], as described in Table S4.

Table S4. Bioclimatic indices used in the geoviticulture climatic classification computed in the Zoning module.

Index	Formula	Classes	Thresholds
Heliothermal or Huglin Index (HI) [38,39]	$$\sum_{1\,April}^{30\,Sept} \frac{(T-T_b)+(T_{max}-T_b)}{2} l_d$$	Very cool	≤ 1500
		Fresh	$1500-1800$
		Temperate	$1800-2100$
		Hot temperate	$2100-2400$
		Hot	$2400-3000$
		Too hot	> 3000
Cool night índex(CNI) [39]	$$\frac{1}{N}\sum_{1\,sept}^{30\,Sept} T_{min}$$	Warm nights	$\geq 18ºC$
		Temperate nights	$14ºC-18ºC$
		Cool nights	$12ºC-14ºC$
		Very cool nights	$\leq 12ºC$
Cool Night Index (CNI_s) [34]	$$\left(\sum_{1\,sept}^{30\,Sept} T_{max}-T_{min}\right)\left(\sum_{1\,sept}^{30\,Sept} N<10ºC\right)$$		
Growing season suitability (GSS) [40	$$\sum_{1\,Jan}^{30\,Sept} N(T>10ºC)$$	Appropriate	> 164
		Favorable	$160-164$
		Very favorable	$151-160$
		Favorable	$147-151$
		Appropriate	< 147
Growing season precipitation (GSP) [40]	$$\sum_{1\,April}^{30\,Sept} P_d$$	Appropriate	> 1021
		Favorable	$972-1021$
		Very favorable	$873-972$
		Favorable	$823-873$
		Appropriate	< 823
Hydrothermal index (Hyd) [31,41]	$$\sum_{1\,April}^{30\,August} (T_{mean}*P_d)$$	Risk of weak contamination	≤ 2500
		Risk of medium contamination	$2500-5100$
		Risk of high contamination	≥ 5000
Mean Thermal Amplitude in September (MTA) [42]	$$\frac{1}{N}\sum_{1\,sept}^{30\,Sept} T_{max}-T_{min}$$	NA	NA
Monthly Dryness Index (DI) [33]	$DI=W_0+P_m-(T_v+E_s)$ $T_v=k_cPET$	Humid	> 150
		Sub-humid	$50-150$

$K_c = -1.184 + 0.01879d_n - 0.00004623{d_n}^2$, R^2 $= 0.66$		Moderate dryness	(-100) – 50
$E_s = \dfrac{PET(1-k)N_{ef\ prec}}{N}$		Accentuated dryness	(-200) – (-100)
$N_{ef\ prec} = monthly\ acumulated\ rain\ in\ mm/5$		Very sharp dryness	≤ (-200)
		Moderate dryness	(-100) – 50

This module uses the Tonietto algorithm [39] to estimate the Potential Sugar Content Index (S, Equation S68). In this index, the Hydrologic Balance (DI) is calculated using the Monthly Dryness Index (DI) according to Table S4. This index considers an initial soil water reserve (W_0) in April and the daily accumulated precipitation (P_d) from April to September, as well as the vegetation transpiration (T_v, Table S4) and the soil evaporation (E_s) for the same period.

Equation S67 uses the reference potential evapotranspiration (PET) determined from the FAO–Penman–Monteith (PM) method recommended by the FAO [43], and the seasonal crop coefficient (K_c) determined based on the quadratic equations of Williams et al. [44] for each day of the year (d_n).

$$S = 239.04 - 0.477\ Flor - 0.171\ DI + 1.025\ (N_{Verai-Matu}) + 1.423\ (T_{Verai-Matu\ 1}) \quad \text{(S68)}$$
$$- 2.110\ (T_{Verai-Matu\ 2})$$

$$T_{Verai-Matu\ 1} : \begin{cases} I > 95\ T_{Verai-Matu\ 1} = T_{Verai-Matu} \\ I \leq 95\ T_{Verai-Matu\ 1} = 22.2ºC \end{cases} \quad \text{(S69)}$$

$$T_{Verai-Matu\ 2} : \begin{cases} I \geq 95\ T_{Verai-Matu\ 2} = 17.1ºC \\ I < 95\ T_{Verai-Matu\ 2} = T_{Verai-Matu} \end{cases} \quad \text{(S70)}$$

$$I = \frac{100 \sum_{1\ july}^{30\ sept} PET}{\sum_{1\ July}^{30\ setp} ETP_{maximum\ of\ each\ month}} \quad \text{(S71)}$$

6. Illness Module

6.1. Powdery Mildew submodule

This submodule was implemented based on the Powdery Mildew Risk Assessment Model developed by the University of California, Davis [1]. This model is derived from epidemiological studies and has been validated across all the grape production areas in California. In this submodule, the meteorological conditions for infections by ascospores and conidia are based on the daily air temperatures during leaf wetness events, as described in Table S5 and Scheme S1. According to the Powdery Mildew Risk Assessment Model, a risk assessment index of 60-100 indicates that the pathogen reproduces every 5 days, whereas an index of 0-30 means that the pathogen reproduces every 15 days [1]

Table S5. Control scheme for the powdery mildew fungus implemented in the *Powdery Mildew submodule* is based on the University of California, Davis Powdery Mildew Risk Assessment Model [1].

Sexual ascospores infection	Period for infection		
$5.5°C < T_{min} < 6.9°C$ and $P \geq 2.5\ mm$	3 days		
$7.0°C < T_{min} < 12.0°C$ and $P \geq 2.5\ mm$	2 days		
$12.1°C < T_{min} < 25.0°C$ and $P \geq 2.5\ mm$	1 day		
Conidial infections—risk assessment	**Germination to conidia**	**Infection**	
$21.1°C < T_{max} < 29.4°C$	In 12 days – if the condition is true 20 points per day in a total of 100 points, if false less 10 points.	**Soft** **Normal** **Heavy**	
		$\leq$ then 30	between	$\geq$ then 60
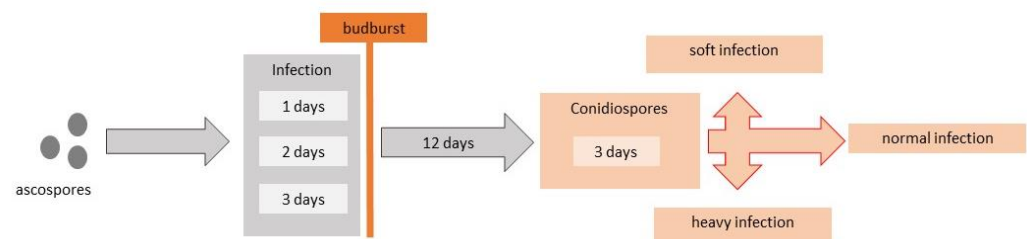
Scheme S1. Conceptualization of the Powdery Mildew submodule.

6.2. Complementary Relationships in Powdery Mildew Epidemics

In the submodule, the relationships between the temperature and germination rate (*GR*, Equation S72), the penetration rate (*PR*, Equation S73), and the reduction in the germination rate (*GMR*, Equation S74) due to the presence of liquid water on the host surface (estimated by Delp [45]), as well as the effect of liquid water on sporulation (*SRM*, Equation S75, estimated by Chellemi [46]), were described by Arafat [47] for the powdery mildew epidemics.

$$GR = -2.641 + 0.256\,T - 0.00528\,T^2 \tag{S72}$$

$$PR = -0.639 + 0.108\,T - 0.00254\,T^2 \tag{S73}$$

$$GMR = 1.155 - 0.014\,T \tag{S74}$$

$$SRM = -10.998 + 0.939\,T - 0.019T^2 \tag{S75}$$

6.3. Downy Mildew submodule

This submodule determines the primary and secondary infections of pseudo fungus downy mildew based on the rule of thumb described by Magarey [48] as outlined in Table S6.

Table S6. The control scheme for downy mildew implemented in the *Downy Mildew submodule* is based on Magarey [48]—Managing Downy Mildew.

1 day	**Oospore germination** $P_d \geq 10\ mm\ and\ T_{min} \geq 8ºC$
	Zoospore realizes and primary infection: $P_d \geq 2.5\ mm\ and\ T_{max} \geq 20ºC$
After 17 days	**Oilspot formation from primary infection**
	Sporangia: $RH \geq 98\%\ and\ T_{min} \geq 13ºC$
Oilspot	**Zoospores realize and second infection:** $P_d \geq 2.5\ mm\ and\ T_{max} \geq 20ºC$
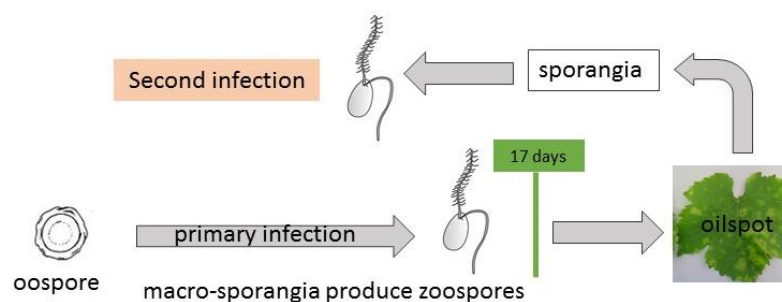
Scheme S2. Conceptualization of the Downy Mildew submodule.

6.4. Delay or advance of downy mildew outbreaks

This submodule calculates the quantification of the delay or the advance of downy mildew outbreaks according to Salinari et al. [49] According to this author, the average date of the first seasonal outbreak and the delay (D) is represented by the linear regressions in Equations S76 to S78.

$$D = -6.061 - 3.686\ DF_1 \tag{S76}$$

$$DF_1 = 0.473\ T_{jan} - 0.142\ T_{Fev} - 0.086\ T_{Marc} + 1.644\ T_{Apri} + 0.754\ CRD_{Marc} \tag{S77}$$
$$+ 0.025\ CND_{Marc} + 0.047\ RD_{Apri} - 23.1$$

$$DF_2 = -0.035\ T_{Jan} - 0.008\ T_{Fev} - 0.663\ T_{Marc} - 0.318\ T_{Apri} \tag{S78}$$
$$+ 0.161\ CRD_{Marc} + 0.104\ CND_{Marc} + 0.106\ RD_{Apri} + 6.5$$

Here, T represents the average daily mean air temperature (ºC) for each month from January to April; CRD_{Marc} represents the maximum number of consecutive rainy days (rain ≥ 0.2 mm) in March; CND_{Marc} represents the maximum number of consecutive days without rain in March; and RD_{Apri} represents the number of rainy days in April.

For $D < 0$, the outbreak of downy mildew is advanced, and for $D > 0, it$ is delayed. DF_1 accounts for 73% of the variability and DF_2 accounts for 27%. The classification of DF_1 and DF_2 is expressed in a discriminant analysis to distinguish the groups of the precocity of the first seasonal outbreaks of grapevine downy mildew (I to III, early to late outbreaks) that occurred in Spresiano (North Italy) from 1980 to 2005, as described in Salinari et al. [49].

7. Interactions between IMVSCA model modules

The IMVSCA system comprises four modules, Light–Shadow, Phenology, Zoning, and Illness. The module Light–Shadow is formed by three submodules: Sunrise–Sunset, Tree–Shadow, and Light–Orchard. In the Sunrise–Sunset submodule, the sunrise and sunset hours are calculated. These hours are integrated with the Tree–Shadow submodule and the Light–Orchard submodule to define the daily period during which a vineyard is influenced by sunlight passing around the tree crown and receiving photosynthetically active radiation. Also, some astrophysics parameters of the Tree–Shadow submodule are calculated using the solar declination simulated by the Sunrise–Sunset submodule.

In the Tree–Shadow submodule, the mean air temperature surrounding a vineyard exposed to daily sunlight and the shadow of the tree are calculated, along with the relative humidity. Both the variables are calculated within the period encompassed by the vegetative and hydrological cycles.

In the Light–Orchard submodule, the photosynthetically active radiation (PAR) received by the vineyards under the shadow of fruit trees, in an orchard configuration, is calculated. This submodule uses the solar azimuth angle, the solar elevation angle at a given hour, the daily extraterrestrial radiation, and the daily global radiation simulated by the Tree–Shadow submodule to calculate the hourly extraterrestrial solar radiation and the hourly incident global solar irradiance.

The two outputs of the Tree–Shadow submodule are integrated with the other observed input variables described in this document within the Phenology, Zoning, and Illness modules.

The interaction between the Tree–Shadow submodule and the Phenology module, as well as the interaction between models in the Phenology module, is described as follows:

- The mean air temperature provided by the Tree–Shadow submodule is used during the vegetative cycle as an input variable to determine the start of vegetative growth in the vineyards under the shadow effect, including budburst, flowering, veraison, maturity, and chilling;

- Regarding phenological phases, when grapevine varieties such as Riesling and Viognier, which produce white wine, Pinot Gris, and Gewürztraminer, which produce rosé wine, and Cabernet Franc, Syrah, and Sangiovese, and which produce red wine, were chosen for analysis, the onset of the phenological phases (flowering, veraison, and maturity) are determined by the accumulation of the mean air temperature starting from the 60th day of the year, according to Parker et al. [21]. Meanwhile, with the other varieties of white grapes such as Alvarinho, Antão Vaz, Arinto, Avesso, Bical, Ratinho, Chardonnay, Encruzado, Fernão Pires, Fonte Cal, Gouveio, Loureiro, Malvasia Fina, Moscatel Graúdo, Rabigato, Sercial, Siria, Verdelho, and Viosinho, and red varieties such as Alfrocheiro, Aragonez, Baga, Castelão, Cabernet Sauvignon, Jaen, Ramsico, Rufete, Tinta Barroca, Tinta Caiada, Tinto Cão, Touriga Franca, Touriga Nacional, Trincadeira, and Vinhão, the onset of the next phenological phase begins after the accumulation of the mean air

temperature reaches a threshold, starting from the onset of the previous phenological phase, as defined by Wang [19] and Lopes et al. [20];

- After the budburst begins, frost control is performed using the relative humidity, along with other input variables provided by the observations as described in this document;

- After the start of flowering, the optimal ranges for pollination and germination are calculated using the relative humidity and mean air temperature, and extreme precipitation events, are determined using accumulated precipitation;

- Scald risk is determined using the relative humidity;

- Both of the variables are used to calculate the Penman–Monteith potential evapotranspiration during the hydrological cycle period;

- After the start of maturation, the temperature accumulation is monitored to determine the onset of chilling in the vineyard in the Phenology module;

- The interaction between the Tree–Shadow submodule, the Phenology module, and Zoning module, is described as follows:

- The Potential Sugar Content Index in the Zoning module is determined using the periods between the onset of the flowering, veraison, and maturation phases simulated in the Phenology module. It utilizes the Penman–Monteith potential evapotranspiration data from the Phenology module, along with other observed variables, to estimate the sugar content in grapes;

- The mean air temperature and relative humidity provided by the Tree–Shadow submodule are used within the hydrological cycle period as input variables for all the indices in the Zoning module that require them;

- The Illness module consists of two submodules: the Powdery Mildew submodule and the Downy Mildew submodule. The interaction between the Tree–Shadow submodule, the Phenology module, and the two submodules of the Illness module is described as follows:

- The Downy Mildew submodule uses the relative humidity data provided by the Tree–Shadow submodule during the vegetative cycle period;

- In the Powdery Mildew submodule, conidiospore control is performed 12 days after the start of vineyard budburst, over the next 3 days.

References

1. Thomas, C.S.; Gubler, W.D.; Leavitt, G. Field testing of a powdery mildew disease forecast model on grapes in California. *Phytopathology* **1994**, *84*, 1070.

2. Nasrin, M.; Chakrabarty, A.; Chandra Barman, M.; Kumar Saha, S.; Nasrin, M.; Kumar Chakrabarty, A.; Mijanoor Rahman, M. Sunrise And Sunset Time Prediction In a Specific Latitude Tracking Selection Criteria of Solar Panels on Consumer Market in Bangladesh View project Fuzzy Numerical Results Derived From Crashing CPM/PERT Networks of Padma Bridge in Bangladesh View project . *IOSR Journal of Mathematics* **2017**, *13*, 1–07, doi:10.9790/5728-1306030107.

3.　Duffett-Smith, P. *Practical astronomy with your calculator*; Third Edit.; Cambridge University Press, 1988;

4.　Duffett-Smith, P.; Zwart, J. *Practical Astronomy with your calculator or spreadsheet*; Cambridge University Press, Ed.; 2017; ISBN 1139495720, 9781139495721.

5.　Hu, L.; Yan, B.; Wu, X.; Li, J. Calculation method for sunshine duration in canopy gaps and its application in analyzing gap light regimes. *Forest Ecology and Management* **2010**, *259*, 350–359, doi:10.1016/j.foreco.2009.10.029.

6.　Angstrom, A. Solar and terrestrial radiation. Report to the international commission for solar research on actinometric investigations of solar and atmospheric radiation. *Quarterly Journal of the Royal Meteorological Society* **1924**, *50*, 121–126, doi:10.1016/0038-092x(63)90167-1.

7.　Hargreaves, G.H.; Samani, Z.A. Estimating potential evapotranspiration. *Journal of the Irrigation and Drainage Division* **1982**, *108*, 225–230.

8.　Doorenbos, J.; Pruitt, W.O. *Guidelines for predicting crop water requirements*; 2nd editio.; Rome, 1977; Vol. 24;.

9.　Castellvi, F.; Perez, P.J.; Villar, J.M.; Rosell, J.I. Analysis of methods for estimating vapor pressure deficits and relative humidity. *Agricultural and Forest Meteorology* **1996**, *82*, 29–45, doi:10.1016/0168-1923(96)02343-X.

10.　Zotarelli, L.; Dukes, M.D.; Romero, C.C.; Migliaccio, K.W.; Morgan, K.T. Step by Step Calculation of the Penman-Monteith Evapotranspiration (FAO-56 Method). *Institute of Food and …* **2010**, 1–10.

11.　Oyarzun, R.A.; Stöckle, C.O.; Whiting, M.D. A simple approach to modeling radiation interception by fruit-tree orchards. *Agricultural and Forest Meteorology* **2007**, *142*, 12–24, doi:10.1016/j.agrformet.2006.10.004.

12.　Campbell, G.S.; Norman, J.M. *An Introduction to Environmental Biophysics*; Springer, Ed.; 2nd ed.; 1998; ISBN 0387949372.

13.　Campbell, G.S. Extinction coefficients for radiation in plant canopies calculated using an ellipsoidal inclination angle distribution. *Agricultural and Forest Meteorology* **1986**, *36*, 317–321, doi:10.1016/0168-1923(86)90010-9.

14.　Chuine, I. A unified model for budburst of trees. *Journal of Theoretical Biology* **2000**, *207*, 337–347, doi:10.1006/jtbi.2000.2178.

15.　Caffarra, A.; Eccel, E. Increasing the robustness of phenological models for Vitis vinifera cv. Chardonnay. *International Journal of Biometeorology* **2010**, *54*, 255–267, doi:10.1007/s00484-009-0277-5.

16.　Hanninen, H. Modelling bud dormancy release in trees from cool and temperate regions. *Acta Forestalia Fennica* 1990, *213*, 1–48.

17.　Sarvas, R. Investigations on the annual cycle of development of forest trees. Autumn dormancy and winter dormancy. *Communicationes. Instituti Forestalis Fenniae.* **1974**, *84*, 1–101.

18.　Mullins, M.G.; Bouquet, A.; Williams, L.E. *Biology of the grapevine*; 1992;

19.　Wang, J.Y. A Critique of the Heat Unit Approach to Plant Response Studies. *Ecologiy* **1960**, *41*, 785–790.

20.　Lopes, J.; Eiras-Dias, J.E.; Abreu, F.; Clímaco, P.; Cunha, J.P.; Silvestre, J. Exigências térmicas, duração e precocidade de estados fenológicos de castas da colecção ampelográfica nacional. *Ciencia e Tecnica Vitivinicola* **2008**, *23*, 61–71.

21.　Parker, A.; de Cortázar-Atauri, I.G.; Chuine, I.; Barbeau, G.; Bois, B.; Boursiquot, J.M. Classification of varieties for their timing of flowering and veraison using a modelling approach: A case study for the grapevine species Vitis vinifera L. *Agricultural and Forest Meteorology* **2013**, *180*, 249–264, doi:10.1016/j.agrformet.2013.06.005.

22.　Gobbett, D.L., Nidumolu, U., Crimp, S. Modelling frost generates insights for managing risk of minimum temperature extremes. *Weather and Climate Extremes* **2020**, *27*, 100176, doi:10.1016/j.wace.2018.06.003.

23.　Poling, E.B. Overview of active frost, frost/freeze and freeze protection methods. In Proceedings of the In Understanding and Preventing Freeze Damage in the Vineyard Workshop Proceedings. Columbia: University of Missouri Extension; 2007; pp. 47–64.

24. Robotham, R.W., Lloyd, J., Warrington, I.J. A controlled environment room for producing advective white or black frost conditions. *Journal of agricultural engineering research* **1978**, *23*, 301–311.

25. Kalma, J.D., Laughlin, G.P., Caprio, J.M., Hamer, P.J. *The bioclimatology of frost: its occurrence, impact and protection*; 2012;

26. Snyder, R. L., Paw U, K. T, Thompson, J.F. Passive frost protection of trees and vines. *DANR Leaflet* **1987**, *21429*.

27. Snyder, R.L; Melo-Abreu, J.D. Frost protection: fundamentals, practice and economics. Volume 1. Frost protection: fundamentals, practice and economics. **2005**, *1*, 1–240.

28. Jones, G.V. The climate component of terroir. *Elements: An International Magazine of Mineralogy, Geochemistry, and Petrology* **2018**, *14*, 167–172.

29. Poling, E.B. Spring Cold Injury to Winegrapes and Protection Strategies and Methods. *HortScience* **2008**, *43*, 1652–1662.

30. Perry, K.B. Guide to deciding when to start and stop irrigation for frost protection of fruit crops. *Horticulture information leaflet 713. New 2/98. North Carolina Cooperative Extension Service. North Carolina State. University College of Agriculture & Life Sciences* **1998**.

31. Magalhães, N. *Tratado de viticultura: a videira a vinha e o terroir*; Esfera Poética, Ed.; 2015; ISBN 9789899820739.

32. Stroe, M.V.; Dunuta, T.V.; Cojanu, D.N. Influence of temperature and humidity in blooming phenophase concerning on fruit set in some table grapes (Vitis Vinifera L). *Scientific Papers-Series B-Horticulture* **2017**, *61*, 269–274.

33. Tonietto, J.; Carbonneau, A. A multicriteria climatic classification system for grape-growing regions worldwide. *Agricultural and Forest Meteorology* **2004**, *124*, 81–97, doi:10.1016/j.agrformet.2003.06.001.

34. Fregoni, M. *Viticoltura di qualità*; L'informat.; 1999;

35. Branas, J.; Bernon, G.; Levadoux, L. *Éléments de viticulture général*; Delmar, Bo.; 1946;

36. Jackson, D. Climate, monographs in cool climate viticulture-2. *Daphne Brasell NZ* **2001**.

37. Blanco-Ward, D.; García Queijeiro, J.M.; Jones, G.V. Spatial climate variability and viticulture in the Miño River Valley of Spain. *Vitis - Journal of Grapevine Research* **2007**, *46*, 63–70.

38. Huglin, M. No Title. *Comptes-rendus de L'Académie d'Agriculture de France* **1978**, *64*, 1117–1126.

39. Tonietto, J. Les macroclimats viticoles mondiaux et l'influence du mesoclimat sur la typicite de la syrah et du muscat de Hambourg dans le sud de la france - méthodologie de caractérisation. **1999**, 233.

40. Sánchez, Y., Martínez-Graña, A. M., Santos-Francés, F., Yenes, M. Index for the calculation of future wine areas according to climate change application to the protected designation of origin "Sierra de Salamanca" (Spain). *Ecological Indicators* **2019**, *107*, 105646, doi:10.1016/j.ecolind.2019.105646.

41. Fraga, H.; Malheiro, A.C.; Moutinho-Pereira, J.; Santos, J.A. Future scenarios for viticultural zoning in Europe: Ensemble projections and uncertainties. *International Journal of Biometeorology* **2013**, *57*, 909–925, doi:10.1007/s00484-012-0617-8.

42. Montes, C.; Perez-Quezada, J.F.; Peña-Neira, A.; Tonietto, J. Climatic potential for viticulture in Central Chile. *Australian Journal of Grape and Wine Research* **2012**, *18*, 20–28, doi:10.1111/J.1755-0238.2011.00165.X.

43. Allen, R.G.; Pereira, L.S.; Raes, D.; Smith, M. *Crop evapotraspiration guidelines for computing crop water requirements.*; 1998; ISBN 9251042195.

44. Williams, L.E.; Phene, C.J.; Grimes, D.W.; Trout, T.J. Water use of mature Thompson Seedless grapevines in California. *Irrigation Science* **2003**, *22*, 11–18, doi:10.1007/s00271-003-0067-5.

45. Delp, C.J. Effect of temperature and humidity on the grape powdery mildew fungus. *Phytopathology* **1954**, *44*, 615–626.

46. Chellemi, D.O. Epidemiology of grape powdery mildew, University of California, Davis, 1990.

47. Arafat, K.H. Application of Statistical Model for Forecasting Powdery Mildew of Grapes under Egyptian Conditions Based on Meteorological Data. *International Journal of Plant Pathology* **2015**, *6*, 48–57, doi:10.3923/ijpp.2015.48.57.

48. Magarey, P.A. *Managing Downy Mildew*; 2010;

49. Salinari, F.; Giosue, S.; Rossi, V.; Tubiello, F.N.; Rosenzweig, C.; Gullino, M.L. Downy mildew outbreaks on grapevine under climate change: Elaboration and application of an empirical-statistical model. *EPPO Bulletin* **2007**, *37*, 317–326, doi:10.1111/j.1365-2338.2007.01126.x.